

Influence of Natural Organic Matter and Ionic Composition on the Kinetics and Structure of Hematite Colloid Aggregation: Implications to Iron Depletion in Estuaries

Steven E. Mylon,^{*,†} Kai Loon Chen,[‡] and Menachem Elimelech[‡]

Department of Chemistry, Lafayette College, Easton, Pennsylvania 18042-1782, and
Department of Chemical Engineering, Environmental Engineering Program,
Yale University, New Haven, Connecticut 06520-8286

Received April 1, 2004. In Final Form: July 13, 2004

The stability and aggregation behavior of iron oxide colloids in natural waters play an important role in controlling the fate, transport, and bioavailability of trace metals. Time-resolved dynamic light scattering experiments were carried out in a study of the aggregation kinetics and aggregate structure of natural organic matter (NOM) coated hematite colloids and bare hematite colloids. The aggregation behavior was examined over a range of solution chemistries, by adjusting the concentration of the supporting electrolyte—NaCl, CaCl₂, or simulated seawater. With the solution pH adjusted so that NOM-coated and bare hematite colloids were at the same zeta potential, we observed a significant difference in colloid stability which results from the stability imparted to the colloids by the adsorbed NOM macromolecules. This enhanced stability of NOM-coated hematite colloids was not observed with CaCl₂. Aggregate form expressed as fractal dimension was determined for both NOM-coated and bare hematite aggregates in both NaCl and CaCl₂. The fractal dimensions of aggregates formed in the diffusion-limited regime indicate slightly more loosely packed aggregates for bare hematite than theory predicts. For NOM-coated hematite, a small decrease in fractal dimension was observed when the solution composition changed from NaCl to CaCl₂. For systems in the reaction-limited regime, the measured fractal dimensions agreed with those in the literature. Colloid aggregation was also studied in synthetic seawater, a mixed cation system to simulate estuarine mixing. Those results describe the important phenomena of iron oxide aggregation and sedimentation in estuaries. When compared to field data from the Mullica Estuary, U.S.A., it is shown that collision efficiency is a good predictor of the iron removal in this natural system.

Introduction

The fate, transport, and bioavailability of trace metals in aquatic environments are specifically linked to their speciation. In oxidic river waters, iron exists primarily as colloidal ferric oxides.¹ The geochemical behavior of these colloids relies not only on their physical properties but also on their surface chemistry. In aquatic environments, one of the most important and studied phenomena involving iron oxide colloids is their aggregation and apparent removal in estuarine mixing zones where saline-rich seawater meets riverine water.^{1–3} The removal of iron in estuaries occurs to such an extent that iron availability is limited in the open ocean. In fact, iron is the only trace metal which has been shown to limit primary production by marine microorganisms.⁴

Past laboratory¹ and field studies² have demonstrated that, as salinity increases in estuaries, the removal of filterable (>0.45 μm) iron begins with colloid aggregation. The complete removal of iron in estuaries requires the

sedimentation of iron aggregates which can be controlled by aggregate form^{5,6} and the residence time of the water in an estuary.⁷ Aggregation phenomena are influenced by factors such as pH, salinity, solution composition, colloid size, surface chemistry, and the concentration of suspended materials or other colloidal aggregates.^{8,9}

To accurately describe the removal of iron oxide colloids in estuaries, it is imperative to first understand the kinetics of aggregate formation in systems representing a natural estuary. While the current body of work describing colloidal aggregation kinetics is quite large,^{10–13} much of it describes model systems that neglect at least one of the many important factors existing in the natural aquatic environments. For example, natural organic matter (NOM) which is ubiquitous in all natural aquatic systems has been shown to adsorb to iron oxide colloids.¹⁴ The adsorbed NOM macromolecules on colloids can change important factors that govern colloid aggregation, such

* To whom correspondence should be addressed. E-mail: mylons@lafayette.edu.

[†] Lafayette College.

[‡] Yale University.

(1) Hunter, K. A.; Leonard, M. R.; Carpenter, P. D.; Smith, J. D. *Colloids Surf., A* **1997**, *120*, 111–121.

(2) Boyle, E.; Edmond, J. M.; Sholkovitz, E. R. *Geochim. Cosmochim. Acta* **1977**, *41*, 1313–1324.

(3) Sholkovitz, E. *Earth Planet. Sci. Lett.* **1978**, *41*, 77–86.

(4) Coale, K. H.; Johnson, K. S.; Fitzwater, S. E.; Gordon, R. M.; Tanner, S.; Chavez, F. P.; Ferioli, L.; Sakamoto, C.; Rogers, P.; Millero, F.; Steinberg, P.; Nightingale, P.; Cooper, D.; Cochlan, W. P.; Landry, M. R.; Constantinou, J.; Rollwagen, G.; Trasvina, A.; Kudela, R. *Nature* **1996**, *383*, 495–501.

(5) Bushell, G. C.; Yan, Y. D.; Woodfield, D.; Raper, J.; Amal, R. *Adv. Colloid Interface Sci.* **2002**, *95*, 1–50.

(6) Johnson, C. P.; Li, X.; Logan, B. E. *Environ. Sci. Technol.* **1996**, *30*, 1911–1918.

(7) Mayer, L. M. *Geochim. Cosmochim. Acta* **1982**, *46*, 1003–1009.

(8) Elimelech, M.; Gregory, J.; Jia, X.; Williams, R. J. *Particle Deposition & Aggregation: Measurement, Modelling and Simulation*; Butterworth-Heinemann: Oxford, 1995.

(9) Mayer, L. M. *Geochim. Cosmochim. Acta* **1982**, *46*, 2527–2535.

(10) Grolimund, D.; Elimelech, M.; Borkovec, M. *Colloids Surf., A* **2001**, *191*, 179–188.

(11) Amal, R.; Coury, J. R.; Raper, J. A.; Walsh, W. P.; Waite, T. D. *Colloids Surf.* **1990**, *46*, 1–19.

(12) van Zanten, J. H.; Elimelech, M. *J. Colloid Interface Sci.* **1992**, *154*, 1–8.

(13) Liang, L.; Morgan, J. J. *Aquat. Sci.* **1990**, *52*, 32–55.

(14) Tipping, E. *Geochim. Cosmochim. Acta* **1981**, *45*, 191–199.

as surface charge characteristics, reactivity, and hydrodynamic radius.^{15,16} Au et al.¹⁷ have attempted to model the complexation and conformation of adsorbed NOM, but their work stops short of modeling the effects of NOM on colloid aggregation. In other work, Amirbahman and Olson^{18–20} demonstrate the effects of NOM on colloid deposition kinetics in porous media comprised of quartz grains. While their work illustrates the importance of adsorbed NOM on colloid attachment efficiency, their systems cannot be used as a model for colloid aggregation in estuaries.

In this work, we employ time-resolved dynamic light scattering (TR-DLS) experiments to study the aggregation kinetics and aggregate structure of NOM-coated hematite colloids and bare hematite. An appropriate comparison of both types of colloids required that we work at the solution pH where the zeta potentials of the colloids are the same. Changing the solution chemistry by adjusting the concentration of the supporting electrolyte—NaCl, CaCl₂, or simulated seawater—allowed us to examine the effects that cations of different valencies have on the rate of colloid aggregation and on aggregate form. Finally, we simulated seawater as the supporting electrolyte and compared aggregation rates across a range of dilutions. The implications of hematite aggregation to iron loss in estuaries are discussed.

Materials and Methods

Colloid Preparation. Hematite (α -Fe₂O₃) colloids were synthesized by the forced hydrolysis of FeCl₃ using the method described by Matijevic and Scheiner.^{21,22} In short, enough FeCl₃·6H₂O was dissolved in hot (100 °C) aqueous 0.002 M HCl to produce a 0.02 M Fe³⁺ solution. After mixing, the container was immediately placed in an oven (100 °C) for 1 week. The resulting sample cooled to room temperature before it was partitioned into smaller aliquots more appropriate for ultra-centrifugation. A cycle consisting of 30 min in an ultra-centrifuge (> 5000g), followed by decanting the supernatant liquid, and then resuspending the colloids in Nanopure™ (18.3 M Ω) water was repeated at least 10 times to ensure the colloids were rid of any excess FeCl₃ or other impurities. Colloids were considered clean and contaminant-free when the conductivity of the supernatant liquid after centrifugation was close to that of deionized water. When all the colloid solutions were clean and contaminant-free, they were combined into one hematite stock solution and aged in an oven at 100 °C for more than 24 h. The pH of the stock solution was 4.75, and the concentration determined gravimetrically was 9.5 ± 0.5 g/L. All solutions used during the synthesis were kept in doubly acid-rinsed high-density polyethylene or Teflon™ bottles to minimize both contact with glass containers and the potential for contamination.

NOM was pre-adsorbed to the hematite colloids using a method similar to that of Amirbahman and Olson.²⁰ In short, a solution of about 185 mg/L Suwannee River humic acid (SRHA; International Humic Substances Society, Golden, CO) was prepared in Nanopure™ water. Hematite colloids (ca. 2 g/L) were added to the SRHA solution, and the pH of the solution was adjusted to 6.2. These conditions were chosen to ensure adequate NOM adsorption while keeping the pH somewhat close to circumneutral so as to best approximate adsorption in natural systems. To

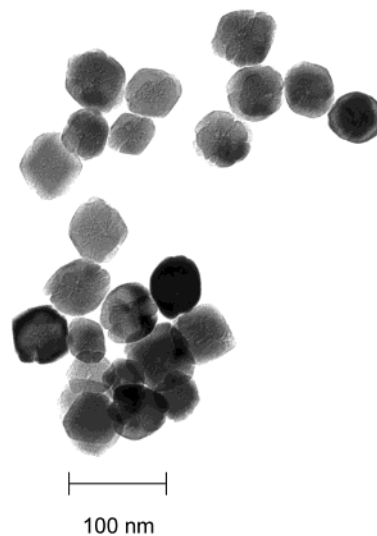


Figure 1. TEM image of the synthesized hematite colloids verifying the sphericity and monodispersity of the colloidal system.

ensure adequate mixing, the colloids were placed on a mechanical shaker for more than 24 h. The sample was centrifuged, and the supernatant liquid was saved for total organic carbon (TOC) analysis by high-temperature oxidation (Shimadzu 5000A). On the basis of this method, we calculated a SRHA adsorption density of 15.2 ± 4.6 (mg C)/g hematite colloids.

Colloid Characterization. The electrophoretic mobility of colloids was measured by microelectrophoresis with phase analysis light scattering (ZetaPALS, Brookhaven Instruments) under solution compositions nearly identical to those used in the aggregation experiments. Zeta potentials (ζ) were determined from the measured electrophoretic mobilities (μ_e) using⁸

$$\mu_e = \frac{\zeta \epsilon f(\kappa a)}{\eta(T)} \quad (1)$$

where $\eta(T)$ is the solution viscosity as a function of absolute temperature T , ϵ is the dielectric constant of water, and $f(\kappa a)$ is a function of particle size, a , and the inverse Debye screening length, κ .

The size and morphology of the hematite colloids were observed by transmission electron microscopy (TEM). Colloids were prepared by first lyophilizing (Labconco, Freezezone 4.5) a portion of the primary hematite solution. The dried colloids were then resuspended in 100% ethanol and placed in an ultrasonic bath for 2 min. One drop (ca. 25 μ L) of the suspension was deposited on a Formvar- and carbon-coated nickel grid (100 mesh), and the ethanol was immediately removed by absorption onto a filter paper, leaving the colloids on the grid. The grid was air-dried and examined in a Tecnai 12 Biotwin electron microscope (FEI) at 100 kV. Images were recorded digitally using a Gatan camera or on film, at magnifications ranging from 68 000 \times to 98 000 \times . An image of these colloids is shown in Figure 1.

Colloid size was also measured by dynamic light scattering (DLS). The instrument consisted of a diode-pumped laser (Verdi V-2/V-5, Coherent) operating at 532 nm, an ALV-SP S/N 30 goniometer (ALV-GmbH, Langen, Germany) with an index matching vat filled with doubly filtered (0.1 μ m) toluene, and an ALV-500 correlator. All measurements were made in dilute suspensions of <5 mg colloid/L. The colloids were pipetted into a cleaned borosilicate vial before measuring the intensity of the auto-correlation function at a 90° scattering angle. The hydrodynamic radius, R_H , was determined by nonlinear least-squares fitting (ALV software) of the resulting second-order cumulants.

Colloid Aggregation. Aggregation rates and resulting stability ratios were determined by a TR-DLS technique similar to the method used by Schudel et al.²³ Dilute colloidal suspensions

(15) Franchi, A.; O'Melia, C. *Environ. Sci. Technol.* **2003**, *37*, 1122–1129.

(16) Tiller, C. L.; O'Melia, C. *Colloids Surf., A* **1993**, *73*, 89–102.

(17) Au, K.-K.; Pennison, A. C.; Yang, S.; O'Melia, C. *Geochim. Cosmochim. Acta.* **1999**, *63*, 2903–2917.

(18) Amirbahman, A.; Olson, T. M. *Environ. Sci. Technol.* **1993**, *27*, 2807–2813.

(19) Amirbahman, A.; Olson, T. M. *Colloids Surf., A* **1995**, *95*, 249–259.

(20) Amirbahman, A.; Olson, T. M. *Colloids Surf., A* **1995**, *99*, 1–10.

(21) Matijevic, E.; Scheiner, P. *J. Colloid Interface Sci.* **1978**, *63*, 509–524.

(22) Raming, T. P.; Winnubst, A. J. A.; van Kats, C. M.; Philipse, A. P. *J. Colloid Interface Sci.* **2002**, *249*, 346–350.

(23) Schudel, M.; Behrens, S. H.; Holthoff, H.; Kretzschmar, R.; Borkovec, M. *J. Colloid Interface Sci.* **1997**, *196*, 241–253.

were titrated to the appropriate pH with either dilute NH_4OH (Seastar) or NaOH (Fisher Scientific), and 1 mL of the pH-adjusted colloid suspension was added to a new cleaned borosilicate vial. To that solution we added the appropriate amount of doubly filtered ($0.2 \mu\text{m}$) NaCl , CaCl_2 , or synthetic seawater (molar ratio $X_{\text{Na}}:X_{\text{Mg}}:X_{\text{Ca}}:X_{\text{K}} = 44.2:5.3:1.1:1$)²⁴ solution. The resulting solution was sealed, given a quick shake, and placed in the index matching vat. Individual autocorrelation functions were successively acquired for between 10 and 15 s over the course of 1–3 h. The calculated hydrodynamic radius from each autocorrelation function represents a mean hydrodynamic radius, R_{H} , taken over a distribution of colloid monomers, dimers, and higher order aggregates.

Initial colloid aggregation kinetics were determined by monitoring the increase in R_{H} with time:²³

$$\left(\frac{dR_{\text{H}}}{dt}\right)_{t \rightarrow 0} \propto kn_0 \quad (2)$$

That is, the product of the aggregation rate constant k and the colloid number concentration n_0 is proportional to the slope of the R_{H} versus time graph for $t \rightarrow 0$. After normalizing the initial slope to the colloid concentration, the inverse stability ratio ($1/W$) can be determined from the ratio of the measured aggregation rate constant, k , to the diffusion-limited (*fast*) aggregation rate constant k_{fast} :

$$\frac{1}{W} = \frac{k}{k_{\text{fast}}} \quad (3)$$

In fact, we can determine $1/W$ without determining the absolute rate constants, because at a fixed n_0 , the ratio of the initial slope of the R_{H} versus time graph to that in the fast regime is proportional to k/k_{fast} :

$$\frac{1}{W} = \frac{(dR_{\text{H}}/dt)_{t \rightarrow 0}}{(dR_{\text{H}}/dt)_{t \rightarrow 0:\text{fast}}} \quad (4)$$

The minimum cation concentration required for diffusion-limited aggregation, the critical coagulation concentration (CCC), was determined by nonlinear least-squares fitting of the empirical relationship between the inverse stability ratio ($1/W$) and the relevant salt concentration $[\text{M}^{n+}]$ according to¹⁰

$$\frac{1}{W} = \frac{1}{1 + (\text{CCC}/[\text{M}^{n+}])^\beta} \quad (5)$$

In this equation, β' is the slope of the $\log(1/W)/\log([\text{M}^{n+}])$ plot in the reaction-limited regime (RLR).¹⁰

The aggregation process results in the formation of fractal aggregates. The fractal dimension (d_f) of the aggregates was calculated from the graph of R_{H} versus time according to a simple power law relationship⁵

$$R_{\text{H}} \propto R_{\text{H}0} t^{1/d_f} \quad (6)$$

where $R_{\text{H}0}$ is the average radius at time $t = 0$.

Results

Colloid Characterization. The mean radius of hematite colloids determined from DLS measurements was $42 \pm 3 \text{ nm}$. For the same hematite colloids, TEM measurements served as a reassuring check of DLS measurements. The colloids appeared mostly spherical (Figure 1) and nearly identical to those synthesized by Zhang and Buffle²⁵ using the same method. To a small extent, the colloids had some angular features, but we made no adjustments to the measured hydrodynamic radii

(24) Schlesinger, W. H. *Biogeochemistry: An Analysis of Global Change*, 2nd ed.; Academic Press: San Diego, 1997.

(25) Zhang, J.; Buffle, J. *J. Colloid Interface Sci.* **1995**, *174*, 500–509.

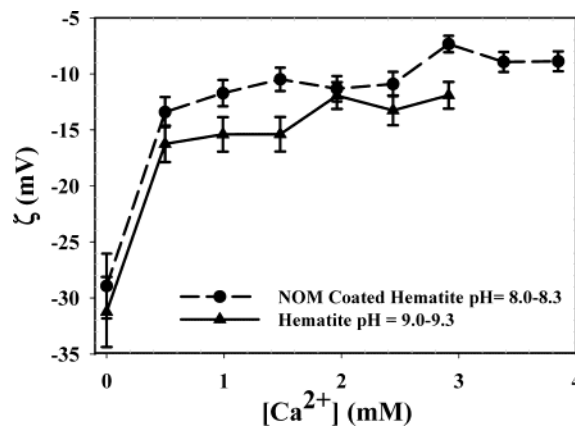


Figure 2. Zeta potentials of colloids across the range of experimental Ca^{2+} concentrations. For the NOM-coated hematite (circles), pH = 8.1, and for the bare hematite (triangles), pH = 9.5. Error bars represent 10% of measured values.

due to these small deviations in the spherical nature of the colloids. Additionally, TEM measurements confirmed that the hematite synthesis produced a monodisperse sample of colloids. From DLS measurements, we were unable to resolve any difference in the hydrodynamic radius of hematite colloids and NOM-coated hematite colloids. This is not surprising because SRHA has an average molecular weight of 10 500 Da¹⁷ and has been suggested to increase the hydrodynamic layer thickness of small ($< 50 \text{ nm}$) hematite colloids by $< 2 \text{ nm}$ at low ionic strengths.¹⁷

Figure 2 shows the calculated zeta potentials of both hematite and NOM-coated hematite colloids across a range of CaCl_2 concentrations. SRHA has a maximum charge density of $-1.35 \text{ C}/(\text{mg carbon})$, and as a result of that negative charge, the colloids coated with SRHA show a more negative zeta potential than the bare hematite when their suspensions are maintained at the same pH.¹⁷ To make useful comparisons between the aggregation behavior of coated and uncoated colloids, the pH of each solution required adjustment so that the zeta potential of the SRHA-coated hematite colloids was equal to that of the bare hematite for each of the aggregation experiments. Figure 2 confirms that by maintaining the pH of the NOM-coated hematite solution at 8.2 ± 0.2 and the pH of the uncoated hematite solution at 9.5 ± 0.2 , the zeta potentials of both types of colloids remain nearly equal.

Figure 2 also shows a decrease in zeta potentials (i.e., less negative) as the CaCl_2 concentration increased. Similarly, when NaCl was used as the background electrolyte, zeta potentials decreased as the ionic strength of the solution increased (figure not shown). The zeta potential measurements of both coated and uncoated hematite colloids in NaCl solution exhibited a similar decrease in zeta potential with increasing electrolyte concentration. At the pH values chosen, we were able to obtain the same zeta potentials for both bare and SRHA-coated hematite across the range of experimental conditions. For hematite a decrease in zeta potential with increases in ionic strength has been observed previously.²⁶

Colloid Aggregation Kinetics. Figure 3 clearly shows that the mean hydrodynamic radius of NOM-coated colloidal aggregates increases with time under most experimental conditions. As the ionic strength of the solution increased, the initial rate of change of the mean R_{H} increased. With small increases in ionic strength, this

(26) Delgado, A. V.; Gonzalez-Caballero, F. *Croat. Chem. Acta* **1998**, *71*, 1087–1104.

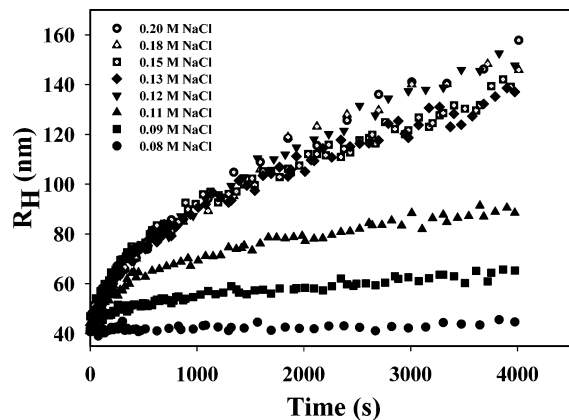


Figure 3. Change in mean hydrodynamic radius of SRHA-coated hematite aggregates with time at pH = 8.2 across a range of NaCl concentrations.

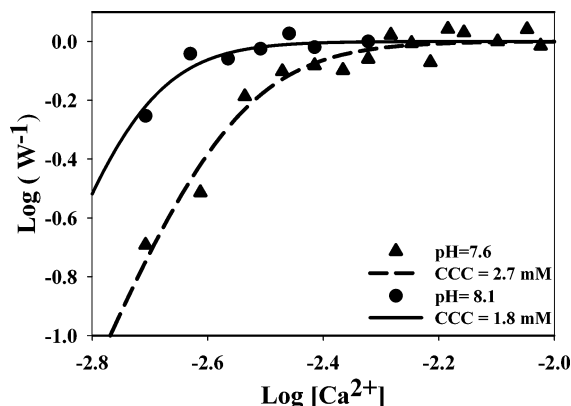


Figure 4. Representative colloidal stability curves for NOM-coated hematite at pH = 7.6 (triangles) and pH = 8.1 (circles). The solid and dashed lines are determined from nonlinear least-squares fitting of the data to eq 5 in the text.

Table 1. CCCs for the Bare Hematite and NOM-Coated Hematite Colloids Using Different Background Electrolytes

colloid system	NaCl (mM)	CaCl ₂ (mM)
uncoated hematite	30	2.4
NOM-coated hematite	107	1.8

trend was observed for both colloid systems (i.e., NOM-coated and bare hematite). From Figure 3, it is clear that the initial rate of change in the mean aggregate R_H increases with electrolyte concentration until a maximum rate of aggregation is reached. As described previously, this diffusion-limited aggregation is reached at a threshold electrolyte concentration known as the CCC. The CCC depends on the specific cation in solution, and under some experimental conditions, the CCC depends on whether the colloids were coated with NOM or were bare. Figure 4 shows representative colloid stability diagrams for a NOM-coated hematite in CaCl₂ at two different pH values. Colloid stability can be characterized by W^{-1} and, under the same experimental conditions, the measured CCC is also a quantitative indicator of colloid stability.

For the uncoated hematite system, the CCC decreased from 30 mM in NaCl to 2.4 mM in CaCl₂. This same trend was observed in the NOM-coated system, but a larger difference existed between the NaCl system, 107 mM, and the CaCl₂ system, 1.8 mM (Table 1). In addition to other cations, simulated seawater contains both Na⁺ and Ca²⁺, and, therefore, the most appropriate manner to compare the colloid stability in seawater is as a function of the ionic strength instead of the ionic concentration. In this

Table 2. Fractal Dimensions of Colloidal Aggregates for the Bare Hematite and NOM-coated Hematite Colloids Using Different Background Electrolytes

colloid system	d_f DLR/NaCl ^a	d_f RLR/NaCl ^a	d_f DLR/CaCl ₂ ^a	d_f RLR/CaCl ₂ ^a
uncoated hematite	1.66 ± 0.11 ^b	^c	1.64 ± 0.11	^c
NOM-coated hematite	1.75 ± 0.14	2.22 ± 0.01	1.66 ± 0.04	2.23 ± 0.07

^a The supporting electrolyte was either NaCl or CaCl₂. ^b Uncertainties were determined using nonlinear least-squares fitting. ^c Fractal dimensions of bare hematite aggregates formed in the RLR are not reported. See discussion in text.

case, we report the critical coagulation ionic strength (CCIS) as a qualitative measure of stability. For the NOM-coated hematite, the CCIS is 80 mM.

Fractal Dimension of Colloid Aggregates. We calculated fractal dimensions (d_f) for each set of experiments. For NOM-coated hematite, the average d_f values were 1.66 ± 0.04 in Ca²⁺ and 1.75 ± 0.14 in Na⁺ for aggregates formed in the diffusion-limited regime (DLR; $[M^{n+}] > \text{CCC}$) and the crossover region ($[M^{n+}] \approx \text{CCC}$), and 2.23 ± 0.01 in Ca²⁺ and 2.22 ± 0.07 in Na⁺ for aggregates formed in the RLR ($[M^{n+}] \ll \text{CCC}$). Because of the steepness of the $d(W^{-1})/d([\text{NaCl}])$ curve in the RLR, more measurements were made in the DLR and in the crossover region than in the RLR. For bare hematite in NaCl, fractal dimensions averaged 1.66 ± 0.11 in the diffusion-limited region and the crossover region. In CaCl₂, d_f averaged 1.64 ± 0.11 in the two regions. For bare hematite, there was a small window of salt concentrations above which aggregation could be measured on a realistic time scale and below which aggregation occurred in the RLR. Because of this, we were limited in the number of measurements we could make in the RLR for this system. With few data points, we were not comfortable reporting the fractal dimensions of these colloidal aggregates formed in the RLR. The fractal dimensions determined for the various experimental conditions employed are summarized in Table 2.

Discussion

Role of NOM in Aggregation Kinetics. The results show that even low molecular weight fractions of NOM, such as humic acids, can enhance colloid stability. By comparing both coated and uncoated hematite at the appropriate pH values to ensure similar electrokinetic properties, we use the CCC as a qualitative measure of colloid stability.²⁷ Figure 5 shows a direct comparison between coated and uncoated hematite in NaCl. While both systems appear to be sensitive to small changes in NaCl concentration, the slope of the curves in the RLR indicates that the coated hematite colloids are nearly three times more sensitive to changes in the electrolyte concentrations. The shift in CCC to higher concentrations of NaCl in the coated hematite system is indicative of the enhanced stability of those colloids.

According to Derjaguin–Landau–Verwey–Overbeek (DLVO) theory, at the CCC the van der Waals attractive interaction is equal to the interaction due to electrostatic repulsion for like-charged spherical colloids. Hence, we can use the experimental CCC values in NaCl to calculate Hamaker constants for both types of colloids and compare them to previously published values for hematite. In a method similar to that of Amal et al.,¹¹ we calculate the Hamaker constant for uncoated hematite to be 1.3×10^{-20} J, which is slightly smaller than that calculated by Amal

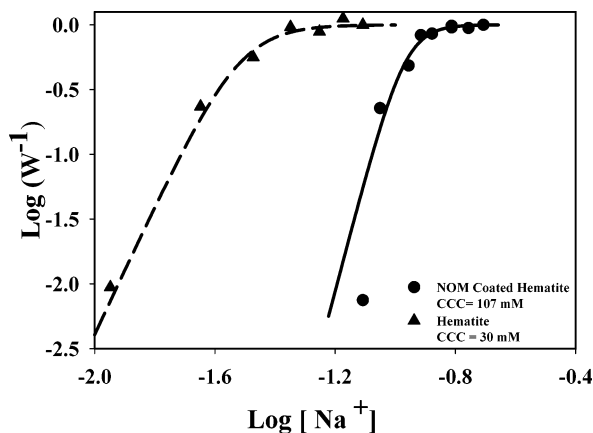


Figure 5. Comparison of SRHA-coated (circles) and bare (triangles) hematite stability in a monovalent (NaCl) salt system. A difference in pH is necessary so that the zeta potentials are kept the same for an appropriate comparison. Aggregation of SRHA-coated hematite colloids can be marginally observed at NaCl concentrations well above the CCC for bare hematite aggregation.

et al.¹¹ However, for the NOM-coated hematite system we calculate the Hamaker constant to be 4.6×10^{-21} J, which is much smaller than any reported value for hematite and clearly unrealistic for any dense metal oxide colloid. Naturally, we should calculate the same or similar Hamaker constants for both systems. However, DLVO theory describes the system by summing the van der Waals and electrostatic interaction energies, and, therefore, the calculated Hamaker constant can be influenced by the enhanced stabilization due to NOM. While the difference in the two calculated Hamaker constants cannot be used to quantify the additional stabilization energy, it indicates, along with the CCC, that NOM does enhance hematite stability in NaCl.

The CCC in CaCl_2 solutions for both systems is smaller than that in NaCl (Table 2). This is to be expected and can be qualitatively predicted by the Schulze–Hardy rule.⁸ For large zeta potentials, the Schulze–Hardy rule predicts $\text{CCC}_{\text{Na}}/\text{CCC}_{\text{Ca}} = 64$, which differs considerably from our measured ratio of 12.5 for the bare hematite system. However, zeta potentials for these colloids are not considerably large and, therefore, the CCC values will scale between z^{-2} , a better predictor at small zeta potentials,²⁸ and z^{-6} . Additionally, the Schulze–Hardy rule is valid for 1:1 and symmetrical electrolytes, which fits the case of NaCl but not CaCl_2 . Accounting for the 1:2 electrolyte decreases the upper limit of this ratio, and, therefore, we consider a ratio of 12.5 to be an appropriate value.²⁸

For NOM-coated hematite, $\text{CCC}_{\text{Na}}/\text{CCC}_{\text{Ca}} \approx 60$, which cannot be accounted for on the basis of the Schulze–Hardy rule alone. The CCCs for both coated and uncoated hematite (Figure 6) are nearly equal in CaCl_2 , and this indicates that there is no measurable steric stabilization due to the NOM coating. The small difference in CCC shown in Figure 6 can result from the uncertainty in zeta potential measurements and other small experimental uncertainties. This lack of enhanced colloid stability in NOM-coated hematite in CaCl_2 can be mistaken for the effect that cation complexation with the SRHA may have on the zeta potential through charge neutralization. However, while Ca^{2+} is known to complex to humic

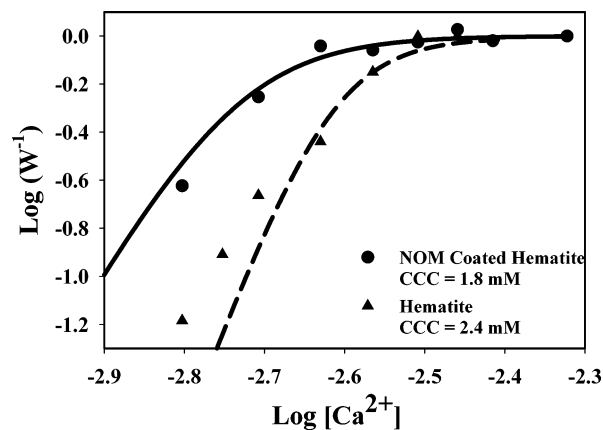


Figure 6. Comparison of SRHA-coated (circles) and bare (triangles) hematite stability in CaCl_2 . The CCCs for both systems are nearly the same, indicating that the NOM coating has little to no effect on colloid stability in CaCl_2 .

substances,²⁹ the zeta potentials of NOM-coated hematite did not reveal any significant reduction with increasing Ca^{2+} concentration when compared to the uncoated hematite (Figure 2). Therefore, our observation that there is no appreciable stabilization of NOM-coated hematite in CaCl_2 cannot be a result of increasingly smaller zeta potentials and, hence, weaker repulsive interactions between these colloids as the Ca^{2+} concentration increases. In fact, for both the coated and uncoated colloids in CaCl_2 , the calculated Hamaker constants are 1.1×10^{-20} J and 1.4×10^{-20} J, respectively, which confirms the observations in the colloid stability diagrams that both systems exhibit nearly identical stability.

As stated above, if significant decreases in zeta potentials resulted from Ca^{2+} complexation to the SRHA, then we would expect to observe a substantial decrease in the stability of NOM-coated hematite in CaCl_2 . Additionally we see no apparent stability enhancement in CaCl_2 , and, therefore, there must be an alternative explanation for our observation that adsorbed SRHA does not impart any additional stability to hematite in CaCl_2 : calcium complexation to the carboxylic acid functional groups of SRHA results in the dehydration of the SRHA, which can enhance the self-association of the humic molecules, thus, limiting their interactions with other colloids. Alternatively, the dehydration of SHRA may cause the humics to spread (flatten) out on the surface of the colloids rather than extend linearly from the surface.³⁰ This too will limit the electrosteric interactions we observed in CaCl_2 . Regardless of the specific mechanism, our results show that, because of this conformational change in the SRHA coating, there is little to no effect on NOM-coated hematite stability in CaCl_2 . Tipping and Higgins³¹ suggest a similar reason for their observations, but having performed their experiments in a solution of SRHA, they observed stability enhancement which is most likely due to additional NOM adsorption to the colloids with increasing CaCl_2 concentration. In our experiments, all NOM is preadsorbed to the hematite, and the concentration of humics that may desorb upon dilution is likely to be small. Therefore, unlike the experiments of Tipping and Higgins, additional adsorption of NOM will not contribute to any appreciable stability as the divalent cation concentration increases.

(29) Hering, J. G.; Morel, F. M. M. *1988*, 22, 1234–1237.

(30) Mosley, L. M.; Hunter, K. A.; Ducker, W. A. *Environ. Sci. Technol.* **2003**, 37, 3303–3308.

(31) Tipping, E.; Higgins, D. C. *Colloids Surf.* **1982**, 5, 85–92.

(28) Hunter, R. J. *Foundations of Colloid Science*; Clarendon Press: Oxford, 1986; Vol. 1.

Influence of NOM on Hematite Aggregate Structure. The short-range forces governing the interactions between spherical colloids influence not only the kinetics of aggregate formation, but also the structure and resulting fractal dimension of the colloid aggregates. The fractal dimensions for aggregates formed in the DLR for NOM-coated hematite are only slightly smaller than those measured in other systems¹¹ or determined from recent theoretical work.^{11,32,33} This agreement justifies our method of fitting the change in R_H with time to a power law function to determine the fractal dimension of aggregates. In the DLR, the fractal dimension of both the coated and uncoated colloids show no differences (Table 2). This observation is not surprising because diffusion-limited aggregate packing is quite loose, and the small molecules associated with SRHA would be unlikely to have an effect on aggregate form during a fast irreversible process.

In the RLR, the fractal dimensions are expected to increase because the colloids have the opportunity to find the lowest-energy aggregate structure, which is the more tightly bound aggregate. Our results show that, in the RLR, the fractal dimensions are slightly larger than those reported by others in other aggregating systems or determined by theoretical modeling. The more tightly bound aggregates responsible for these larger fractal dimensions may occur because, as the colloids aggregate, the van der Waals attraction between adsorbed SRHA on adjacent colloids can result in an even tighter structure than the aggregates formed from uncoated hematite. More interesting is the small difference in fractal dimensions of NOM-coated hematite aggregates in different electrolytes formed in the DLR. Others have postulated that charge neutralization and not colloid bridging determines aggregate form in the DLR.²⁵ The small difference that we observe may be explained by the complexation of calcium with SRHA and its potential to bridge between colloids. Aggregation through this mechanism should result in a more loosely packed aggregate, which is in contrast to the system where the supporting cation (Na^+) is not known to complex SRHA and, therefore, aggregation is not enhanced by the bridging of colloids. While recognizing this speculative nature of this mechanism for aggregation, it does offer a simple explanation based on the observed physical and chemical properties of the system components.

It is important to mention that our procedure of fitting the growth of the R_H to a power law function may not be appropriate in the RLR.³⁴ In these cases, fractal dimensions need to be determined through other techniques such as static light scattering. This suggests the need for a comparison between two methods of fractal dimension determination—fitting a power law function to a plot of R_H versus time and the more conventional method of static light scattering.⁵ The results of such work should be more conclusive as to the effects of NOM coating on the hematite colloids on the fractal dimensions of colloidal aggregates.

Implications to Iron Removal in Estuaries. Our experiments using synthetic seawater as a background electrolyte show that mixed cation systems have an effect on the colloid stability intermediate between solutions containing only monovalent cations and those containing only divalent cations. This trend agrees with that observed by Grolimund et al.¹⁰ in the aggregation of a soil-derived colloidal system. To provide further insights into iron oxide

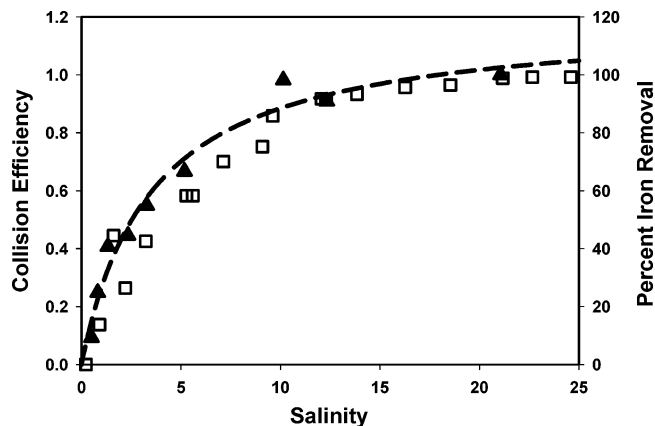


Figure 7. Collision efficiency (inverse stability ratio) as a function of salinity (described in text) based on experimental results (triangles) for NOM-coated hematite colloids in simulated seawater. This illustrates that the rate of colloid aggregation approaches its maximum in the earliest portion of the mixing zone ($S \approx 12$). Field data (open squares) from Boyle et al.² in the Mullica Estuary, New Jersey, U.S.A. (10/13/75), show that total iron concentrations can decrease by 80–90% where the salinity reaches 12.

aggregation in natural waters, we created a model estuary by performing experiments in increasingly more concentrated samples of synthetic seawater. In effect, this served to simulate the longitudinal mixing of freshwaters with saline-rich ocean waters. As described earlier, the molar cation ratio in the synthetic seawater stock solution, $X_{\text{Na}}:X_{\text{Mg}}:X_{\text{Ca}}:X_{\text{K}}$, was 44.2:5.3:1.1:1.

Figure 7 shows the results of aggregation experiments (solid triangles) with NOM-coated hematite in this model estuary. Instead of overall salt concentration, we use salinity (S) because it accounts for both the concentrations and valence states of all the cations (Na^+ , K^+ , Ca^{2+} , and Mg^{2+}) in solution, and salinity is a more commonly used measure of salt content in estuaries and seawater than ionic strength or specific conductance. Salinity is a dimensionless measure and can be calculated from the ionic strength of the solutions.^{35,36} For comparative purposes, salinity generally ranges from 0 in freshwater to 36 in the open ocean, and in our system, the composition of a solution with a salinity of 15 was 0.22 M Na^+ , 0.026 M Mg^{2+} , 0.005 M Ca^{2+} , and 0.005 M K^+ . Additionally, common for aggregation studies in natural waters, we express colloid stability in terms of collision efficiency, which is simply the inverse of the stability ratio. A collision efficiency of 1 indicates that each collision between particles results in attachment, as is expected in diffusion-limited aggregation.

Figure 7 clearly shows that the aggregation rate of NOM-coated hematite is primarily influenced by salinity changes in the earliest portion of an estuarine mixing zone. The DLR for these colloids is reached relatively quickly, and the efficiency of colloidal aggregation is unity.

Notwithstanding important physical parameters of estuarine mixing such as the residence time of water within an estuary, the removal of filterable iron also depends on both the aggregation rate of iron oxide colloids and on the settling rate of these aggregates. On the basis of both experimental and theoretical calculations, aggregates with larger fractal dimensions will settle at faster rates than those with smaller fractal dimensions.⁶ There-

(32) Weitz, D. A.; Huang, J. S.; Lin, M. Y.; Sung, J. *J. Phys. Rev. Lett.* **1985**, *54*, 1416–1419.

(33) Lin, M. Y.; Lindsay, H. M.; Weitz, D. A.; Klein, R.; Ball, R. C.; Meakin, P. *J. Phys.: Condens. Matter* **1990**, *2*, 3093–3113.

(34) Zhou, Z.; Wu, P.; Chu, B. **1991**, *146*, 541–555.

(35) Snoeyink, V. L.; Jenkins, D. *Water Chemistry*; John Wiley & Sons: New York, 1980.

(36) Millero, F.; Sohn, M. L. *Chemical Oceanography*; CRC Press, Inc.: Boca Raton, 1992.

fore, those aggregates formed when the salinity is still quite low (collision efficiency < 0.4 , Figure 7) will have a tendency to settle faster than those formed at higher salinities when aggregation kinetics are controlled by diffusion. However, as a result of the slower aggregation kinetics during regions of low salinity, these faster settling rates will not control the overall process of iron removal.

The implications of NOM adsorbed to colloids on the removal of iron in natural waters is clear from the associated plot (open squares) in Figure 7. The data from Boyle *et al.*² show the percent of iron removal as a function of salinity in the Mullica estuary in New Jersey, U.S.A. In their study, iron removal was determined by measuring the total iron in the filtrate ($> 0.45 \mu\text{m}$) of samples taken longitudinally across the Mullica estuary. The correlation between the experimental results in our model estuary and the field data is remarkably good. In both our

simulated estuary and the Mullica estuary, the rate of colloid aggregation approaches its maximum in the earliest portion of the mixing zone where the salinity $S \approx 12$. The corresponding field data specifically show that total dissolved iron concentrations can decrease by as much as 80–90% by the time $S = 12$. On the basis of our data, collision efficiency alone is a very good predictor of the decrease in dissolved iron in the Mullica estuary, and we suggest that it can be used as a tool for modeling iron oxide aggregation and iron removal in estuaries.

Acknowledgment. The authors gratefully acknowledge financial support from the NSF (BES 0228911) and the Henry and Camille Dreyfus Postdoctoral Program in Environmental Chemistry (support of S.E.M).

LA049153G